ELKHA : Jurnal Teknik Elektro, Vol. 15 No.2, October 2023, pp. 139 - 145
ISSN: 1858-1463 (print), 2580-6807 (online)

Computer Aided Classification of X-ray Images from Pediatric Pneumonia Subjects Collected in Developing Countries

Yusuf A Amrulloh[1*)], Bayu D Prasetyo[2)], Ummatul Khoiriyah [3)], Hesti Gunarti[4)], Dwikisworo Setyowireni[5)], Rina Triasih[6)], Roni Naning[7)], and Amalia Setyati[8)]

[1, 2] Department of Electrical Engineering, Universitas Islam Indonesia, Indonesia
[3)] Faculty of Medicine, Universitas Islam Indonesia, Indonesia
[4, 5, 6, 7, 8)] Department of Pediatrics, Universitas Gadjah Mada/Dr Sardjito Hospital, Indonesia
Corresponding Email: [*)] yusuf.amrulloh@uii.ac.id

***Abstract* – Pneumonia is a lower tract respiratory infection due to bacteria or viruses. It is a severe disease in the pediatric population. Pneumonia is the leading cause of mortality in children under five years worldwide. One of the problems with pneumonia is the diagnosis, as the symptoms of pneumonia may overlap with other diseases, such as asthma and bronchiolitis. In this work, we propose to develop a method for classifying pneumonia and non-pneumonia using X-ray images. We collected 60 X-ray images from Dr. Sardjito Hospital, Yogyakarta, Indonesia, and the dataset from Kaggle. We processed these images through pre-processing algorithms to enhance the image quality, segmentation, white pixel computation, and classification. The novelty of our method is using the ratio of the white pixels from edge detection using the Canny algorithm with the white pixels from segmentation for classifying pneumonia/non-pneumonia. In the Kaggle dataset, our proposed method achieved an accuracy of 86.7%, a sensitivity of 100%, and a specificity of 85%. The classification using the dataset from Dr. Sardjito Hospital yields sensitivity, specificity, and accuracy of 80%, 60%, and 66.7%, respectively. Despite the low performance in the results, we proved our novel feature, ratio of white pixels, can be used to classify pneumonia/non-pneumonia. We also identified that the local dataset is essential in the algorithm development as it has a different quality from the dataset from modern countries. Further, our simple method can be developed further to support pneumonia diagnosis in resource-limited settings where the advanced computing devices or cloud connection are not available.**

Keywords: Classification, x-ray images, segmentation, edge detection, white pixels, pediatric pneumonia.

I. INTRODUCTION

The lungs are one of the critical organs in humans. They are responsible for gas exchange in the human metabolism[1]. Pollution, bacteria, or viruses can affect the organ's condition by causing infection or inflammation [2]. In the community, children are more prone to respiratory diseases than adults due to their developing immune systems. An extra concern is required to protect the children's population from respiratory diseases.

Recently, air quality become an essential issue in some cities in Indonesia. The dry season and pollution drive the air quality life index (AQLI) in some cities, such as Jakarta, shot up and became one of the worst in the world [3]. The air quality issue is critical as it can affect the condition of the lungs. Long-term exposure to pollution is stated to be more dangerous than smoking [4]. Further, pollution to children can impact their cognitive and neurodevelopment, asthma, impaired lung function [5]. The World Health Organization (WHO) stated that every day, around 93% of children under fifteen years of age inhale polluted air that is dangerous for their health [6]. The data show that around 600 thousand children died from respiratory diseases [6]. In Indonesia, respiratory diseases have become one of the leading causes of mortality in children under five years of age [7]. Of those mortality cases, around 80-90% were caused by pneumonia, which can also be triggered by air pollution [8].

Pneumonia is a respiratory disease due to bacteria, viruses, or fungi. It can cause alveoli inflammation, where the alveolar sacks are filled with fluid. The condition makes oxygen and carbon dioxide exchange blocked, as such the oxygen level in the blood declines. Furthermore, it leads to rapid breathing and chest indrawing, the common symptoms of pneumonia [9]. These symptoms are used in the integrated management of children's illnesses (IMCI) issued by WHO to establish diagnosis of pneumonia in remote areas [10]. However, these symptoms may also exist in other lower respiratory diseases, hence, can lead to overdiagnosis and unnecessary antibiotic prescription [11].

The chest x-ray is suggested as the gold standard to support the diagnosis of pneumonia [12]. In Indonesia, the government aims to provide X-ray machines in the first-level health facilities (Puskesmas), which the rural population can access. However, only some of the first health facilities are supported by radiologists. Therefore, in the condition where the radiologist is absent, an automated method for classifying pneumonia is required.

Several studies have proposed automated pneumonia

Manuscript received 2023-09-08; revised 2023-10-03; accepted 2023-10-05

classification to address the issues. Previous research investigated the implementation of the algorithm of CNN (convolution neural network), KNN (k-nearest neighborhood), Random Forest, XGBoost, AdaBoost, GradientBoost, and Decision Tree for pneumonia classification [13]. They achieved accuracy from 86% to 98%. The highest accuracy was obtained using the CNN algorithm. The implementation of deep neural networks was also reported in [14]–[19]. The accuracy achieved by these studies was between 96% to 99%. Unfortunately, all those methods require a high computational device that is not always available in remote areas. Furthermore, all studies used overseas data collected from developed countries (Guangzhou Women and Children Medical Centre and The Global Library of Women's Medicine). The dataset is available in Kaggle [20]. There was no study using datasets collected from developing countries such as Indonesia. The data from the latter country often has substandard quality due to the skill of the operator or the quality of the X-ray machine [21]. The substandard X-ray image may affect the interpretation and classification of the results.

In this work, we study pneumonia and non-pneumonia classification using data collected from Indonesia and developed countries (Kaggle). The contributions of our study are:

i) We proposed a simple image processing method to classify pneumonia and non-pneumonia. In this method, we used the ratio of white pixels from edge detection using the Canny algorithm with white pixels from the output image from segmentation. Its simplicity becomes the novelty of our work. Unlike deep neural networks, our algorithm requires only a standard computing device.

ii) We used a dataset from Indonesia and identified their technical problems.

iii) We compare the results of classification between the Indonesia and Kaggle datasets.

In the following sections, we describe the study's methods, results, discussion, and conclusion.

II. METHODOLOGY

A. Dataset

We collected sixty X-ray images for this study. Thirty of these datasets were collected from the Dr. Sardjito Hospital, Yogyakarta, Indonesia. Ethical clearance for this data collection had been approved before the study began. A radiologist examined the dataset and classified it into pneumonia (P) and non-pneumonia (NP). Unfortunately, the number of datasets of the two classes was not equal due to the existing condition in the hospital. The non-pneumonia class consisted of 20 datasets, while the pneumonia class consisted of 10 datasets.

An equal number of datasets were collected from Kaggle [20]. The diagnosis of the diseases had been provided along with the dataset. In this work, we denote the data from Sardjito Hospital as Dataset A, data from Kaggle as dataset B, and combined data as dataset C. We processed all the datasets through image processing sequences described in the following sections.

Figure 1 illustrates the block diagram of the procedure used in this study. The X-ray images were processed through four stages: pre-processing, segmentation, combination and white pixel computation, and classification.

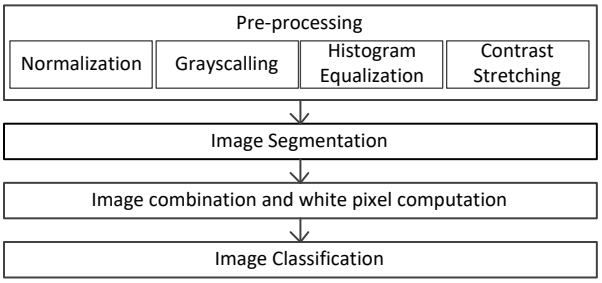

Figure 1. The algorithm of this study comprised of pre-processing, segmentation, image combination and white pixel computation, and classification.

B. Image Pre-processing

The pre-processing consisted of four steps: normalization, grayscalling, histogram equalization, and contrast stretching [22]. We used digital x-ray images in joint photographic expert group (jpeg) format as input. The image is a continuous function of light intensity on two-dimensional planes following Equation (1).

$$f(x,y) = \begin{bmatrix} f(0,0) & \cdots & f(0,M-1) \\ f(1,0) & \cdots & f(1,M-1) \\ \vdots & \vdots & \vdots \\ f(N-1,0) & \dots & f(N-1,M-1) \end{bmatrix} \quad (1)$$

where N is the row, and M is the column of the pixel.

First, the input image was processed through normalization. In this process, the input images, which had different sizes of pixel, were standardized into 256x256 pixels. Later in the grayscalling process, the output images from normalization were turned into gray by following Equation (2).

$$f_o(x,y) = (f_i^R(x,y) + f_i^G(x,y) + f_i^B(x,y))/3 \quad (2)$$

where f_i^R, f_i^G, and f_i^B re the degree of gray function for red, green, and blue color pixel i, respectively.

The output images from grayscalling were then processed into histogram equalization. In this stage, we equalized the distribution of gray color level following the probability function as stated in Equation (3).

$$p\_x\,(i) = p(x = i) = n\_i\,/\,(n, 0 \le i < L) \quad (3)$$

where L is the total number of gray levels in the image (L = 256), and n is the total number of pixels in the image.

Lastly, the pixel values of the images were mapped to a wider range to enhance the contrast. We aimed to improve the details and features of the X-ray image. We follow Equation (4) for this process.

$$s(x,y) = \left({}^{(r(x,y) - r_{max})}/_{r_{min} - r_{max}} \right) \times 255 \quad (4)$$

where s is the updated pixel intensity value, while r is the current pixel intensity value. The r_{min} and r_{max} are the minimum and maximum intensity values present in the whole image.

C. Segmentation

The segmentation process was aimed to get the lungs area out of the images. In this process, we implemented the Chan-Vese segmentation algorithm [23]. This algorithm is based on iterative sets of growth levels to minimize energy, determined by weighted values corresponding to the sum of magnitude differences from the mean outside the region, the sum of the differences from the mean in the segmented region, and a term that depends on the length of the boundary of the segmented region. The energy function of Chan-Vese (CV) is presented in Equation (5).

$$\begin{aligned} E^{CV}(c_1, c_2, C) = {} & \mu.length(C) + v.area(C) + \\ & \lambda_1 \int_{in(C)} |s(x,y) - c_1|^2 dxdy + \\ & \lambda_2 \int_{out(C)} |s(x,y) - c_2|^2 dxdy \end{aligned} \quad (5)$$

where C is the segmentation curve, c_1 is the average intensity in the contour, c_2 is the average intensity outside the contour. Parameters λ_1 and λ_2 were used to control image intensity inside and outside the contour, while parameter μ was used to control the smoothness of zero level set.

After the segmentation process, the value of pixel at (x,y) position in the image is notated as in Equation (6).

$$I_{seg}(x,y) = \begin{cases} 0 & I_{BW}(x,y) < E^{CV} \\ 1 & I_{BW}(x,y) \geq E^{CV} \end{cases} \quad (6)$$

where I_{BW} is the value of grey pixel at (x,y) position.

D. Combination and white pixel computation

In this stage, we combined the image output from the pre-processing and the output from the segmentation processes following Equation (7). This combination was expected to reveal the opacity of x-ray image due to the respiratory diseases.

$$P_{comb}(x,y) = s(x,y).I_{seg}(x,y) \quad (7)$$

The image from the combination was then sent to edge detection. In this study we implemented Canny edge detection algorithm [24]. There were four steps process in the edge detection includes: i) noise reduction, ii) the image's intensity gradient calculation, iii) non-maximum suppression, and iv) hysteresis thresholding.

E. Classification

The classification is intended to distinguish between the x-ray images of pneumonia and non-pneumonia. In this process, we computed the ratio of white pixel of the image from the edge detection and the image from the segmentation process following Equation (8).

$$Q = \delta \,/\, \sigma \quad (8)$$

where δ is the number of white pixels in the image from edge detection and σ number of white pixels in the image from segmentation process.

To check the effectivity of the algorithm we computed the accuracy, sensitivity, and specificity as shown in Equation (9) to Equation (11).

$$accuracy = \frac{TP+TN}{TP+TN+FP+FN} \quad (9)$$

$$sensitivity = \frac{TP}{TP+FN} \quad (10)$$

$$specificity = \frac{TN}{TN+FP} \quad (11)$$

where TP is true positive, TN is true negative, FP is false positive, and FN is false negative. We also computed receiver operating characteristic (ROC) curve as well as area under the curve (AUC).

For programming we use Matlab software installed a laptop with intel i-7 microprocessor, 8GB RAM, and 256 GB SSD.

III. Results and Discussion

In this section, we present the results of this study according to the steps in the method's sections.

A. Dataset

This study included sixty X-ray images from pediatric subjects, wherein thirty data were from Dr Sardjito Hospital (Dataset A) and the rest were from Kaggle (Dataset B). A radiologist examined the dataset from Dataset A to see its quality. Some technical problems were found from the examination, such as low contrast, incomplete inspiration, and rotation. Complete inspiration means that the subject did not inhale the air properly; as such, the lung did not inflate full enough before the image was taken. Meanwhile, rotation is the condition where the subject moves concerning the medial axis during the photograph.

Table 1. Identification Of Dataset From Dataset A

Category	Quantity
Low contrast	6
Incomplete inspiration	3
Rotation	2
Normal	19

We show the information on dataset quality in Table 1. There are six low-contrast images, three incomplete inspirations, and two rotation images, while nineteen images were good in quality. The data from Kaggle showed better quality and was free from technical problems.

Figure 2 illustrates the comparison of pediatric X-ray images from Dr Sardjito Hospital (A) and from Kaggle (B). The first figure has a lower contrast compared to the second image. In Figure 3, we illustrate the image samples from Dataset A that have poor contrast, incomplete inspiration, and rotation. All these types of data were included in this study to gain information about their effects on the classification.

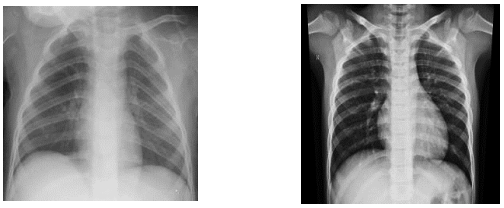

(A) (B)

Figure 2. (A) A typical x-ray image from Dataset A and (B) a typical x-ray image from dataset B.

(A) (B) (C)

Figure 3. Illustration some technical problems in the dataset (A) poor contrast, (B) incomplete inspiration, and (C) rotation.

B. Image processing

The results of image processing are shown in Figure 4 and Figure 5. Each of these figures contains six images (A to H). Image A is the original jpeg file used as input, B is the output from normalization having 256x256 pixels, C is the output from grayscalling, D is the output from histogram equalization, E is the output from contrast stretching, F is the output from segmentation, G is the combined image of segmentation and contrast stretching, and H is the output from edge detection.

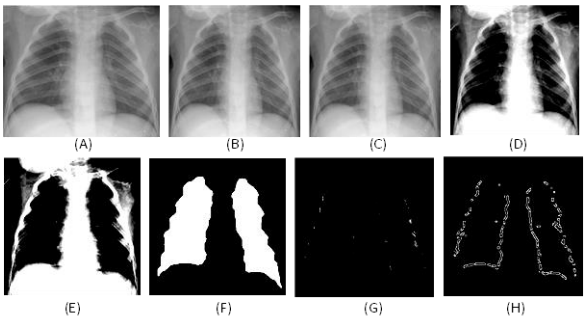

Figure 4. Illustration of image processing using x-ray image from non-pneumonia subject. A is image input, B is normalization output, C is grayscalling output, D is histogram equalization output, E is contrast stretching output, F is segmentation output, G is combined image, H is edge detection output.

Figure 4(E) shows the output of contrast stretching from non-pneumonia subjects. In the figure, the part of the lung has a solid black color, and when segmented, the lungs have a solid white area with the black background, as shown in Figure 4(F). The combination of these figures (Figure 4(E) and Figure 4(F)) shows opacity only at the edge of the lungs, as illustrated in Figure 4(G) and Figure 4(H).

Nonetheless, in pneumonia subjects, the output from contrast stretching shows a white area inside the lungs. Hence, whenever the image was combined with the segmentation output, it showed the opacity inside the lung area, as illustrated in Figure 5(G) and Figure 5(H). The opacity in the lung area indicates the solidification. In pneumonia, solidification is caused by the inflammation of the alveolus that makes them filled with fluid or phlegm. This condition reduces the capacity of the lungs, decreases the oxygen levels, and leads to rapid breathing. These are the common symptoms in children with pneumonia.

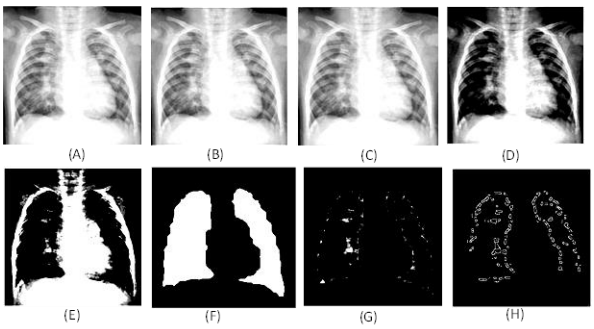

Figure 5. Illustration of image processing using x-ray image from pneumonia subject. The description of A to H is similar to Figure 4.

C. Classification

To distinguish X-ray images of pneumonia and non-pneumonia subjects, we quantify the opacity in the lung area by counting the number of white pixels. We also computed the white pixel from the area of lungs from the segmentation process.

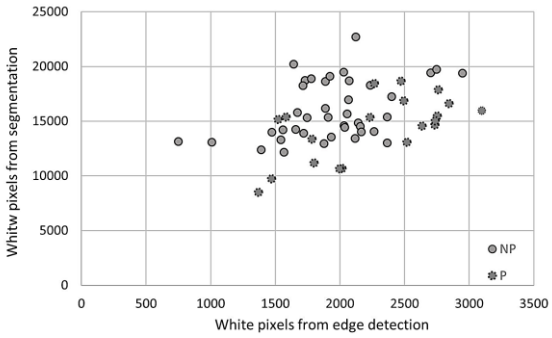

Figure 6. Plotting of the number of white pixels from edge detection against the number of white pixels from segmentation. NP = non-pneumonia, P = pneumonia.

We illustrate the results of the white pixel computation in Figure 6, wherein the x-axis is the number of white pixels from edge detection, and y-axis is the number of white pixels from segmentation. Most of the data are overlapping as such this information cannot be implemented directly. However, statistical analysis found

that the mean of white pixel number from edge detection in non-pneumonia (1,934.5) is lower than in pneumonia (2,254.3). In contrast, the mean of the white pixel number from segmentation in non-pneumonia is higher than in pneumonia (1,5982.2 and 1,4361.7, respectively). Similar results were found in the first and third quartiles, as shown in Figure 7.

As described in the method sections, we computed the ratio of the number of white pixels from edge detection and the number of white pixels from segmentation. This method was used since the pneumonia image contains opacity that can be revealed in the edge detection. In some pneumonia images, the area of the lungs was also smaller than normal. As such, the comparison was expected to create a feature that can be used for simple classification.

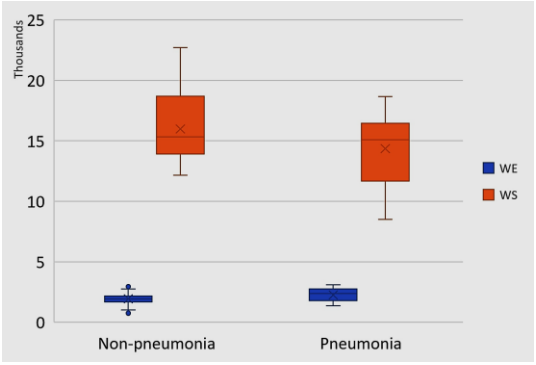

Figure 7. Statistical analysis of white pixel from edge detection (WE) and white pixel from segmentation (WS) in non-pneumonia and pneumonia.

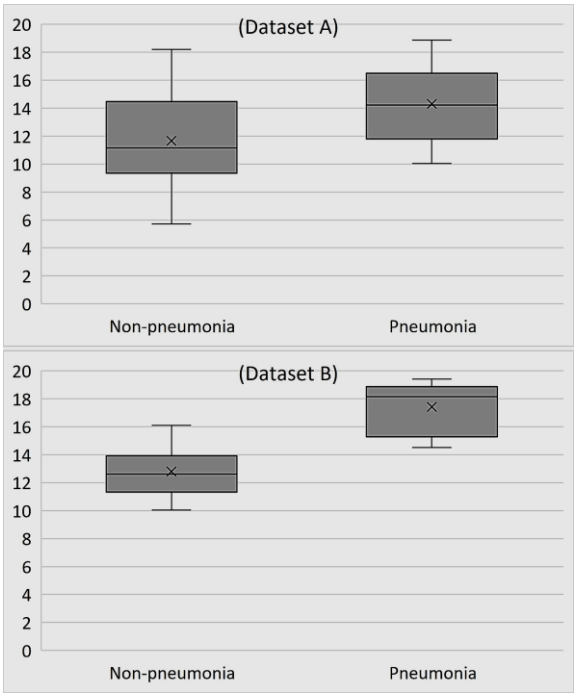

Figure 8. Statistical analysis of ratio between the number of white pixels from edge detection and segmentation. It shows the difference between non-pneumonia to pneumonia. Dataset A was from Dr. Sardjito Hospital, dataset B was from kaggle.

The statistical information of the ratio of the number of white pixels from edge detection and the number of white pixels from segmentation is illustrated in Figure 8. In the later discussion, we denote it as a ratio only. The figure shows that in both Dataset A and, specifically Dataset B, the ratio has different statistical values.

In Dataset A, we see an overlapping distribution between the ratio in pneumonia and non-pneumonia. However, we can notice that some statistical values are different. The non-pneumonia median is lower than pneumonia (11.2 and 14.2, respectively). The average of ratio for non-pneumonia is also lesser than pneumonia (11.7 compared to 14.3). Further, non-pneumonia's first and third quartiles (Q1 and Q3) are 9.3 and 14.3. These numbers are much lower compared to pneumonia (Q1 = 11.8, Q3 = 16.5).

A similar trend occurs in Dataset B wherein the median in non-pneumonia is significantly less than in pneumonia (12.6 and 18.1). The average of ratio in non-pneumonia is also lesser than pneumonia by 4.6 points. Further, the first and third quartiles (Q1 and Q3) for non-pneumonia are 11.3 and 13.9. The numbers are much lower compared to pneumonia (Q1 = 15.3, Q3 = 18.9). Dataset C (a combination of Dataset A and B) shows similar statistical results wherein the minimum, maximum, median, mean, Q1, and Q3 of ration in non-pneumonia are relatively much lower compared to ratio in the pneumonia dataset. The complete statistical data is shown in Table 2.

Table 2. The Statistical Data of Ratio White Pixel From Edge Detection and Segmentation. NP = Non-Pneumonia, P = Pneumonia, Min = Minimum, Max, Maximum, Q1 = 1st Quartile, Q3 = 3rd Quartile, IQR = Interquartile Range.

Parameter	Dataset A		Dataset B		Dataset C	
	NP	P	NP	P	NP	P
Min	5.7	10.0	10.1	14.5	5.7	10.0
Max	18.2	18.9	16.1	19.4	18.2	19.4
Median	11.2	14.2	12.6	18.1	12.2	16.1
Mean	11.7	14.3	12.8	17.4	12.2	15.9
Q1	9.3	11.8	11.3	15.3	10.4	13.6
Q3	14.5	16.5	13.9	18.9	14.2	18.5
IQR	5.1	4.7	2.6	3.6	3.8	4.9

The classification was carried out by using the ratio and category of diseases (non-pneumonia and pneumonia. We computed the receiver operating characteristic (ROC) and area under the curve (AUC). Then, we also computed the accuracy, sensitivity, and specificity of classification results following Equation (9) – (11).

Figure 9 illustrates the ROC curve of Dataset A. The AUC, sensitivity, specificity, and accuracy of data set A are 0.735, 80%, 60%, and 66.7%, respectively. The AUC is higher than 0.5. This means the classification result is significant and not random estimation only. Those parameters were achieved with a threshold of 11.64. The excellent classification results are shown in Dataset B, as illustrated in Figure 10. The classification results show AUC of 0.965, a sensitivity of 100%, a specificity of 85%,

and an accuracy of 86.7% with a threshold of 14.52.

The significant difference between Dataset B to Dataset A can be affected by the quality of the datasets. In section B, we previously described that Dataset A suffers some technical problems such as low contrast, incomplete inspiration, and rotation. These technical problems made the output from segmentation and edge detection less optimum.

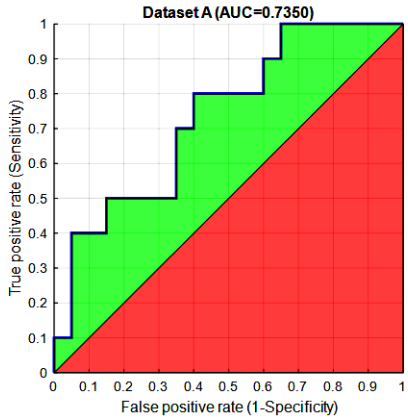

Figure 9. The ROC of dataset A.

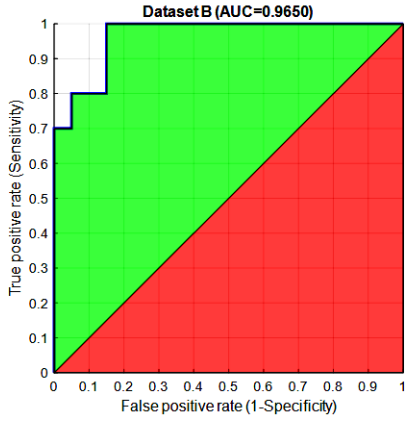

Figure 10. The ROC of dataset B.

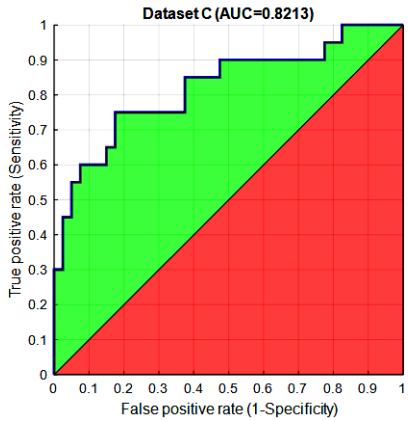

Figure 11. The ROC of dataset C.

In the combined dataset (Dataset C), the usage white pixels ratio results in AUC, sensitivity, specificity, and accuracy of 0.821, 75%, 82.5%, and 80%, respectively, at a threshold of 14.47. These parameters indicate that the classification is a good test. The combination of datasets made the results slightly lower than in the classification in Dataset B as it contains data with technical problems. The ROC curve of Dataset C is illustrated in Fig 11, and the performance parameters is presented in Table 3.

Table 3. The Classification Results of Dataset A, Dataset B, and Dataset C. AUC = Area Under Curve, Sens = Sensitivity, Spec = Specificity, Acc = Accuracy.

	AUC	Sens (%)	Spec (%)	Acc (%)
Dataset A	0.735	80	60	66.7
Dataset B	0.965	100	85	86.7
Dataset C	0.821	75	82.5	80

The accuracy achieved in our study is lesser compared to studies in [13]–[19]. The maximum accuracy in our study is 86% while the existing studies varies from 86% to 99%. However, there are important aspects make our work incomparable. First, we included the dataset from Indonesia. This dataset had not been studied in those previous studies. All those studies used datasets taken in modern countries. As such, our findings have not been explored before. Second, we proposed a simple pneumonia and non-pneumonia classification method by computing the ratio of white pixels from edge detection from the combined image and image from the segmentation. This method requires an average computing device. On the contrary, the studies that used deep learning require an advanced graphic processing unit (GPU), memory, as well as a central processing unit (CPU). Lastly, we investigated the technical problems that exist in the dataset from developing countries. Our results showed that classification using the typical dataset yields lower performance.

Despite the promising results, our study is limited by the number of datasets (60 subjects) in which the proportion of pneumonia and non-pneumonia imbalance. This occurred due to the availability of a dataset from the hospital when we started this study. Future work should be carried out using a larger dataset with an equal proportion of each class. Hence, the findings of the study will be more conclusive.

IV. Conclusion

This study presents the work on paediatric pneumonia and non-pneumonia classification using X-ray images. In this work, we proposed a novel method by quantifying the ratio of white pixel from edge detection of a combined image and white pixel from segmentation process. Our approach to derived the new ratio feature is new as majority of the existing studies use the whole image and let artificial intelligent for classification. Hence, the most contributing feature cannot be known. We tested the algorithm in three datasets namely dataset A from Indonesia, dataset B from developed country (Indonesia), and dataset C the combination of the two datasets. The algorithm achieved the maximum performance in dataset

B (sensitivity of 100%, specificity of 85%, and accuracy of 86.7%) and the minimum performance in Dataset A (sensitivity of 80%, specificity of 60%, and accuracy of 66.7%). The difference performances were caused by the technical problems found in dataset A such as rotation, poor contrast, and incomplete inspiration. Compared to pneumonia classification using deep neural network (DNN), our method achieved lower accuracy. However, those studies have not tested using dataset from Indonesia that suffer technical problems as described previously. The technical problems affected the classification results, and this has not been studied before. This finding emphasizes the importance to include local dataset in the development of classification algorithm. Another advantage of our method, it can be implemented in a standard computing device. On the contrary, DNN requires high performance computing resources. Therefore, our methods can be implemented in the limited-resource areas to support the pneumonia diagnosis where the radiologists are absent and computing device and cloud access are not available.

ACKNOWLEDGEMENT

The authors would like to thank to Dr. Sardjito Hospital and DPPM UII for their support in this study.

REFERENCES

[1] A. Davies and C. Moores, *The Respiratory System: Basic Science and Clinical Condition*, 2nd ed. Edinburgh: Churcill Livingstone, 2010.

[2] H. J. Zar and T. W. Ferkol, "The global burden of respiratory disease-Impact on child health," *Pediatric Pulmonology*, vol. 49, no. 5, pp. 430–434, May 2014.

[3] IQAir, "Air quality in Jakarta." Accessed: Sep. 01, 2023. [Online]. Available: https://www.iqair.com/indonesia/jakarta

[4] M. Wang *et al.*, "Association Between Long-term Exposure to Ambient Air Pollution and Change in Quantitatively Assessed Emphysema and Lung Function," *JAMA*, vol. 322, no. 6, p. 546, Aug. 2019.

[5] J. Medrano, N. Crnosija, R. W. Prather, and D. Payne-Sturges, "Bridging the environment and neurodevelopment for children's health: Associations between real-time air pollutant exposures and cognitive outcomes," *Frontiers in Psychology*, vol. 13, Oct. 2022.

[6] WHO, "Air Pollution and Children Health," Switzerland, 2018.

[7] Balitbangkes, *Laporan Nasional Riskesdas 2018*. Jakarta: Lembaga Penerbit Badan Penelitian dan Pengembangan Kesehatan, 2018.

[8] X. Zhou *et al.*, "Associations between air pollutant and pneumonia and asthma requiring hospitalization among children aged under 5 years in Ningbo, 2015–2017," *Frontiers in Public Health*, vol. 10, Jan. 2023.

[9] A. T. Ebeledike C, *Pediatric Pneumonia. [Updated 2023 Jan 16]. In: StatPearls [Internet]*. Treasure Island (FL): StatPearls Publishing, 2023.

[10] W. H. Organization, "Handbook : IMCI integrated management of childhood illness." World Health Organization, p. Previously issued as WHO document WHO/FCH/CAH/00.1, 2005.

[11] J. Lawrence, L. Andrew, A. Voskoboynik, J. Bracken, and H. Hiscock, "14 Overdiagnosis of pneumonia leading to unnecessary antibiotic use in bronchiolitis," in *Evidence Based Medicine*, BMJ Publishing Group Ltd, Dec. 2019, p. A13.2-A13.

[12] T. A. Florin and J. S. Gerber, "Sticking by an Imperfect Standard: Chest Radiography for Pediatric Community-Acquired Pneumonia," *Pediatrics*, vol. 145, no. 3, p. e20193900, Mar. 2020.

[13] R. E. Al Mamlook, S. Chen, and H. F. Bzizi, "Investigation of the performance of Machine Learning Classifiers for Pneumonia Detection in Chest X-ray Images," in *2020 IEEE International Conference on Electro Information Technology (EIT)*, IEEE, Jul. 2020, pp. 098–104.

[14] J. Hou and T. Gao, "Explainable DCNN based chest X-ray image analysis and classification for COVID-19 pneumonia detection," *Sci Rep*, vol. 11, no. 1, pp. 1–15, 2021.

[15] T. Rajasenbagam, S. Jeyanthi, and J. A. Pandian, "Detection of pneumonia infection in lungs from chest X-ray images using deep convolutional neural network and content-based image retrieval techniques," *J Ambient Intell Humaniz Comput*, no. 2016, 2021.

[16] M. F. Hashmi, S. Katiyar, A. W. Hashmi, and A. G. Keskar, "Pneumonia detection in chest X-ray images using compound scaled deep learning model," *Automatika*, vol. 62, no. 3–4, pp. 397–406, 2021.

[17] H. Agrawal, "Pneumonia Detection Using Image Processing And Deep Learning," in *2021 International Conference on Artificial Intelligence and Smart Systems (ICAIS)*, IEEE, Mar. 2021, pp. 67–73.

[18] R. Alsharif, Y. Al-Issa, A. M. Alqudah, I. A. Qasmieh, W. A. Mustafa, and H. Alquran, "Pneumonianet: Automated detection and classification of pediatric pneumonia using chest x-ray images and cnn approach," *Electronics (Switzerland)*, vol. 10, no. 23, 2021.

[19] M. Yaseliani, A. Z. Hamadani, A. I. Maghsoodi, and A. Mosavi, "Pneumonia Detection Proposing a Hybrid Deep Convolutional Neural Network Based on Two Parallel Visual Geometry Group Architectures and Machine Learning Classifiers," *IEEE Access*, vol. 10, pp. 62110–62128, 2022.

[20] D. S. Kermany *et al.*, "Identifying Medical Diagnoses and Treatable Diseases by Image-Based Deep Learning," *Cell*, vol. 172, no. 5, pp. 1122-1131.e9, Feb. 2018.

[21] F. Zennaro *et al.*, "Digital Radiology to Improve the Quality of Care in Countries with Limited Resources: A Feasibility Study from Angola," *PLoS ONE*, vol. 8, no. 9, p. e73939, Sep. 2013.

[22] R. C. González and R. E. Woods, *Digital Image Processing*, 4th ed. New York: Pearson, 2018.

[23] T. F. Chan and L. A. Vese, "Active contours without edges," *IEEE Transactions on Image Processing*, vol. 10, no. 2, pp. 266–277, 2001.

[24] J. Canny, "A Computational Approach to Edge Detection," *IEEE Transactions on Pattern Analysis and Machine Intelligence*, vol. PAMI-8, no. 6, pp. 679–698, 1986.